Synchrotron Infrared Microspectroscopy: A New Technique for Probing the Chemical Composition of Bone and its Implications for Understanding Osteoarthritis

L. M. Miller, D. Hamerman, and M.R. Chance (Albert Einstein Center for Synchrotron Biosciences), G. L. Carr and G. P. Williams (NSLS), Cathy S. Carlson (Bowman Gray School of Medicine)

Osteoarthritis is the leading cause of disability among people over 65 years old and affects approximately 40 million people in the United States (Center for Disease Control, 1990). It is characterized by a breakdown of the articular cartilage and thickening of the subchondral bone. To date, the cause of osteoarthritis is unknown, but, an extensive study of cynomolgus monkeys has demonstrated that the subchondral bone thickening precedes the development of articular lesions.[1] In addition, a recent study on humans determined that the subchondral bone from patients with symptomatic osteoarthritis was hypomineralized compared with that from asymptomatic individuals.[2] These data suggest that the health and integrity of the articular cartilage is dependent upon the mechanical properties of the underlying subchondral bone. In turn, the mechanical properties of subchondral bone are also dependent upon its chemical structure.

Over a lifetime, bone is continuously remodeling itself and the chemical composition of bone is extremely important to this process. Chemically, bone is made up of both organic and mineral components. The organic component is primarily type I collagen, whereas hydroxyapatite, $Ca_{10}(PO_4)_6(OH)_2$, is the mineral component of bone. As bone matures, the size, crystallinity, and stoichiometry of the hydroxyapatite crystals change. Substitutions into the hydroxyapatite crystal lattice are common, where calcium can be replaced by cations such as Na^+, K^+, Mg^{2+}, Sr^{2+}, and Pb^{2+}. Phosphate and hydroxide can be replaced by CO_3^{2-}, HPO_4^{2-}, Cl^-, and F^-. These substitutions into the hydroxyapatite lattice are very important to bone strength, flexibility, and the process of remodeling because they affect crystal size, density, and solubility. Thus, we hypothesize that the bone matrix composition and/or bone mineral content and crystallinity are modified *in situ* in a specific manner as a function of subchondral bone thickness.

We have addressed this hypothesis by examining the chemical composition of subchondral bone using *infrared micro-spectroscopy*. Infrared spectroscopy is an analytical technique that is sensitive to the chemical components in bone. This technique can be used to determine (1) protein structure and concentration, and (2) mineral concentration, crystallinity, and content (e.g. phosphate, acid phosphate, carbonate). The crystallinity results are correlated to hydroxyapatite crystal size and perfection, as determined by x-ray powder diffraction. By putting infrared light through a microscope, infrared spectra can be collected on micron-sized regions of bone *in situ* and compared to visible images of the same region. Thus, we can examine the chemical composition of subchondral bone as a function of subchondral bone thickness, i.e. severity of osteoarthritis.

Inherently, the long wavelengths of infrared light limit the spatial resolution achievable with this technique. We have demonstrated that substantial changes in chemical composition occur within 20 μm of the site of new bone growth.[3, 4] This type of spatial resolution can only be achieved with a *synchrotron* infrared source. Beamline U4IR at the National Synchrotron Light Source provides the world's brightest source of synchrotron infrared light — 1000 times brighter than a conventional

infrared source — permitting rapid data collection at the diffraction limit, i.e. 3-5 μm in the mid-infrared region. Recently, we used synchrotron infrared microspectroscopy to examined the subchondral plate of a knee joint from a radiographically normal cynomolgus monkey (Miller *et al.*, 1997a, b). The results can be summarized as follows: (1) Bone crystallinity decreases and (2) the carbonate / phosphate ratio increases as subchondral bone thickens. (3) The phosphate / protein ratio is high where crystallinity is high. (4) The acid phosphate concentration is relatively constant throughout the subchondral bone. Since these results suggest that the chemical composition of subchondral bone varies with thickness, we hope that future experiments as a function of disease severity will continue to provide a chemical understanding of the molecular basis for subchondral bone thickening in osteoarthritis. ■

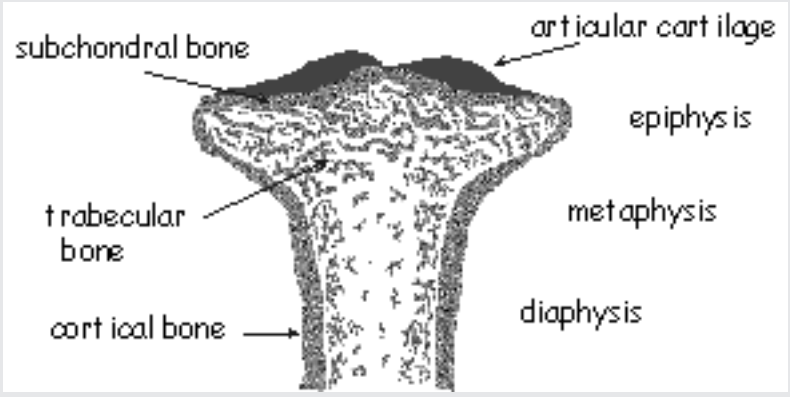

Figure I-1: Schematic drawing of the proximal end of a monkey tibia.

[1] C.S. Carlson, R.F. Loeser, C.B. Purser, J.F. Gardin, C.P. Jerome, "Osteoarthritis in cynomolgus macaques III: Effects of age, gender, and subchondral bone thickness on the severity of disease", *J. Bone & Mineral Res.* 11: 1209-1217 (1996).

[2] B. Li, R.M. Aspden, "Mechanical and material properties of the subchondral bone plate from the femoral head of patients with osteoarthritis or osteoporosis", *Ann. Rheum. Dis.* 56: 247-254 (1997).

[3] L.M. Miller, C.S. Carlson, G.L. Carr, G.P. Williams, M.R. Chance, "Synchrotron infrared microspectroscopy as a means of studying the chemical composition on bone: Applications to osteoarthritis", *SPIE*, 3153: 141-148 (1997).

[4] L.M. Miller, C.S. Carlson, G.L. Carr, M.R. Chance, "A method for examining the chemical basis for bone disease: Synchrotron infrared microspectroscopy", *Cell. and Mol. Biol.*, in press (1997).

Macromolecular Crystallography Area Detectors

L. Berman (NSLS)

During the 1997 fiscal year, the area detectors for all of the macromolecular crystallography beamlines were upgraded, or were in the process of being upgraded. The overall intention was to make the collection of crystallography data to be a less laborious and more user-friendly chore, and to reduce the fraction of users' beam time (dead time) in which no data could be collected at all.

Beamline X4A, operated by HHMI, had installed a Rigaku R-Axis IV automatic imaging plate detector, replacing the manual Fuji imaging plates with off-line readout. The new detector contains two plates, allowing one plate to be read out (in about 3 minutes) while the other is exposing. This allows more efficient use to be made of the available beam time and simultaneously reduces the necessary labor to run the experiment, because manual exchange, readout, and erasure of imaging plates (with the concomitant book-keeping) are no longer necessary. Beamline X4C, also operated by HHMI and undergoing commissioning, will, when operational, use an Area Detectors Systems Corp. (ADSC) Quantum-1 single-module, 1Kx1K CCD detector, which has a readout time of less than 10 seconds.

Beamline X8C, whose PRT was recently reconstituted under the principal auspices of Los Alamos National Laboratory, re-commenced a macromolecular crystallography program using the X-Ray Research (MAR) 300 mm diameter automatic imaging plate system that had been used on the X12C (BNL Biology Dept.) beamline for several years. This single-plate detector has a full-area readout time of about 3 minutes. On beamline X9B, under the joint auspices of the Albert Einstein College of Medicine and the National Institutes of Health, a MAR 345 mm diameter automatic imaging plate system was implemented. This new single-plate detector has a full-area readout time of under 1.5 minutes.

Beamline X12B, operated by the BNL Biology Dept., had earlier in the year removed the MAR 300 mm diameter imaging plate detector, that had been in use there, from its base. It was remounted on the long two-theta arm in the experimental hutch, that was historically employed for small angle x-ray scattering experiments. This upgrade allowed for having a very long detector distance (so that large unit cell crystals could be studied) and, by tilting the two-theta arm, attaining high resolution. An ADSC Quantum-4 four-module CCD detector (1Kx1K per module), funded by the 1996 DOE Basic Energy Sciences Facilities Initiative Program along with some contributions by a few pharmaceutical companies, was also ordered for X12B, and arrived at the start of the 1998 fiscal year.

On X12C, also operated by the BNL Biology Dept., a single-module, 1Kx1K CCD detector, built by a collaboration of Brandeis U. and the BNL Biology Dept., was installed at the start of the 1997 fiscal year. It was presented as an optional alternative to the MAR 300 mm diameter imaging plate detector which had been in use on X12C for several years. The bulk of the macromolecular crystallography experiments on X12C have been serviced by the CCD detector since. At the start of the 1998 fiscal year, a four-module CCD detector was delivered by the Brandeis / BNL Biology collaboration to X12C for commissioning. It will ultimately be made available for use on X25.

On the X25 wiggler beamline, operated by the NSLS, a new MAR 345 mm diameter imaging plate system, provided by the NSLS via Facilities Initiative Program funds, was installed to service macromolecular crystallography experiments. This replaced use of two different MAR 300 mm diameter imaging plate systems, loaned during the past few years to X25 by the BNL Biology Dept. and Cold Spring Harbor Laboratory. The readout time of the new detector (per unit plate area) is 3 times faster than for the old MAR detectors, and it has a finer spatial resolution. In addition, a MAR single-module, 2Kx2K CCD detector, with even finer spatial resolution and a readout time of less than 10 seconds, was also funded by the NSLS via the Facilities Initiative Program, and its delivery is expected in the 1998 fiscal year. It will be able to substitute on X25 for the MAR imaging plate detector, on the same mounting base, when desired. The use of this CCD detector will not be restricted to macromolecular crystallography. Finally, the Brandeis / BNL Biology four-module CCD detector mentioned above that was commissioned on X12C, will become available for use on X25 during early 1998.

Beamline X26C, primarily operated in the past with focussed and unfocussed white x-ray beam capabilities, for Laue macromolecular crystallography and other white beam experimental programs, by the University of Chicago Consortium for Advanced Radiation Sources (CARS) and the BNL Applied Science and Biology

Departments, got an NSLS-sponsored upgrade to give it a standard monochromatic beam capability. Cold Spring Harbor Laboratory and the State University of New York at Stony Brook joined this PRT in the 1997 fiscal year, and began a monochromatic macromolecular crystallography experimental program, based upon a MAR 300 mm diameter imaging plate system provided by Cold Spring Harbor. This system replaced the manual Fuji imaging plates that had been provided by CARS for several years. ■

Nearly Automatic Macromolecular Crystallography at the NSLS

T. Terwilliger, J. Berendzen (Los Alamos National Laboratory),
J. Skinner, R. Sweet (BNL Biology Department)

The pace of protein-structure determination is accelerating rapidly, and synchrotron X-ray sources such as the NSLS are at the center of this action. Structures of protein molecules are in high demand in biotechnology because they are important for applications such as drug discovery and engineering enzymes for commercial use. A structure of a protein molecule can be used to identify what each part of the molecule is doing and makes it possible to design new protein molecules that have improved properties for therapeutic or industrial use. As the genome projects continue to produce thousands of new protein sequences, the demand for structural information on these proteins is increasing. Synchrotron beam lines are a key tool for protein structure determination. The multiwavelength anomalous diffraction (MAD) method takes advantage of the intensity and tuneability of x-rays from synchrotron radiation sources in obtaining x-ray diffraction data that can be used to solve protein structures that contain atoms with accessible x-ray absorption edges.

Until recently, the measurement and analysis of MAD x-ray data has been somewhat difficult owing to the number of steps involved and to the need for an expert to make important decisions about how to handle the data. We have assembled a variety of software and hardware systems to do much of this work for inexperienced users. These include beamline-control and data-collection software, graphical monitoring of data reduction, remote monitoring of beamline operations, and automatic solving of the phase problem to produce an electron-density map of the macromolecule.

The portions of this that involve acquisition of the data, developed by Skinner and Sweet, have been produced for the operation of the synchrotron beamline X12C at the NSLS. These were highlighted in the 1996 NSLS Activity Report. Users of the beamline communicate with all the experimental apparatus, including both the data-collection equipment and the beamline components including the monochromator, through an easy-to-use graphical user interface (GUI). Important features of the system are (1) its modularity, so that different underlying programs or different apparatus can be incorporated easily, (2) its ease of use, minimizing both user errors and training effort, and (3) that most of the experimental operations and parameters are logged automatically, again minimizing errors and facilitating more-or-less automatic reduction of the data. At the time of writing, several different area-sensitive detectors are available (see accompanying article by L. Berman) for mounting on the four-circle diffractometer at the beamline.

The logging of experimental parameters allows the nearly automatic reduction of data. We have constructed a graphical diagnostic routine to display color-coded information about the course of data reduction, neearly all of which is performed while users are present at the beamline. A web-based (Java code) tool monitors much of the information that is displayed on the GUI at the beamline, allowing beamline staff and professors back home to keep track of the course of the data collection at the beamline. Portions of this software package are in use at several beamlines, and we expect to be able to disseminate it further.

To close the loop on the nearly automatic solving of structures, a new software package called SOLVE developed by Terwilliger and Berendzen can carry out all the steps and make all the necessary decisions in the analysis of MAD data automatically, and we have installed

it at beamlines X12C, X8C, and X4A at the NSLS. The SOLVE software has now been run by a number of users at these beamlines and has proven itself capable of solving protein structures in less time than was necessary to collect the x-ray data.

SOLVE is an expert system that automatically produces three-dimensional electron-density maps of protein molecules from x-ray diffraction measurements. For a MAD structure determination, a user at the NSLS will measure diffraction intensities from a single crystal at several x-ray wavelengths spanning an absorption edge for an anomalously scattering atom, such as selenium, incorporated into the protein. These are the raw data needed by SOLVE. The user tells SOLVE where these data are located, what the scattering properties of the selenium atoms are at the x-ray wavelengths used, how many selenium atoms are thought to be in the protein, and how big the protein is. SOLVE takes this information and constructs an electron density map that can be displayed using a graphics program.

The approach used by SOLVE is similar to the one that a protein crystallographer would use. The MAD method for structure determination is a kind of bootstrapping operation in which the positions of the anomalously scattering atoms are first deduced and then used to calculate electron density for the entire structure. The hard part is coming up with likely solutions for the positions of the heavy atoms and evaluating the relative quality of different solutions. These steps often have been done manually in the past, while SOLVE can carry them both out automatically. SOLVE generates a list of likely solutions for the locations of the heaviest atoms in the protein using the program HASSP to analyze an optimized Patterson function derived from the MAD data with MADBST. It then evaluates each solution for internal consistency and it compares characteristics of the electron density map obtained from that solution with those of real electron density maps of proteins. Using the best starting solutions, SOLVE bootstraps to generate improved solutions, and when further improvement is not possible produces a final electron density map of the protein molecule.

Several additional features make SOLVE much faster than it otherwise would be and enable real-time structure solving. One, the MADMRG procedure, is a technique for extracting the three essential pieces of information from a set of up to MAD diffraction measurements. Another, the origin-removed patterson refinement procedure in HEAVY, reduces calculation time by rapidly adjusting a solution to match the x-ray measurements.

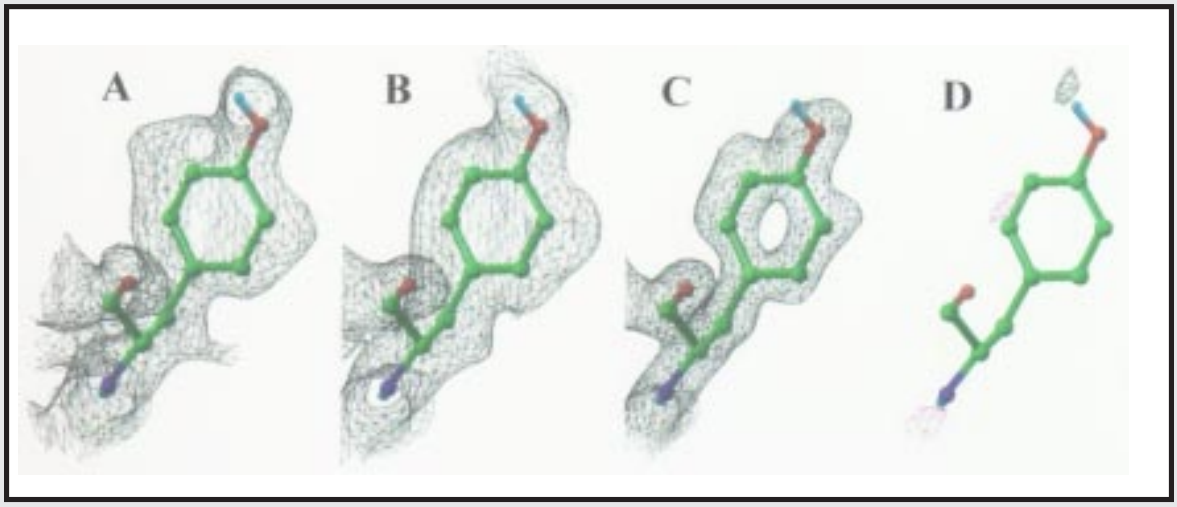

Figure I-2: Electron density maps from MAD-phased MkH data around tyrosine 108. All electron density maps are contoured at 1.5 σ except for D.
(A) 2.0 Å electron density obtained using phases from SOLVE.
(B) 2.0 Å electron density after solvent flattening and histogram matching.
(C) 1.5 Å, 2 fo-fc electron density from current model.
(D) Difference electron density (fo-fc) contoured at 3.0 σ. Positive difference density is contoured in grey and negative density is contoured in black.

Bayesian Correlated MAD Phasing, is a comprehensive way to deal with errors in measurement and to deal with large differences between crystals used in the diffraction analysis. The result of this integration of techniques is a fully automated analysis of x-ray diffraction measurements.

The recent successful structure determination by Richard Fahrner, Duilio Cascio and David Eisenberg (UCLA) at X12C illustrates how useful SOLVE can be. The UCLA group was interested in determining the structure of a histone protein (HMK) from a thermophilic organism. After other methods of solving the structure failed, they used established methods for selenomethionine incorporation to produced selenomethionyl histone protein, and then obtained crystals of the protein. Late in 1997, they came to beamline X12C at the NSLS to collect data for a three-wavelength MAD experiment. Since accurate anomalous information is required for a good MAD experiment, they collected anomalous pairs using the Friedel flip method: for every wavelength there were two datasets, sweeping the same zones, 180 degrees apart. Their MAD experiment consisted of six complete datasets; two at the rising inflection point of the absorption spectrum (0.9798 Å), two at the "white line" peak (0.9799 Å), and two at a distant point (0.9500 Å). Data collection proceeded smoothly and rapidly, employing the automatic MAD data-collection protocols described above. Two factors accelerated high resolution data collection. The size and dynamic range of the new four-module Brandeis CCD-based detector permitted collection of high resolution and low resolution data in a single pass. Also, careful orientation of the crystal with respect to the major zones allowed collection of a large amount of data in a short period of time. The integrated data were about nine-fold redundant, greater than 99% complete to 1.4 Å, with a merging R of 8.1%. Data collection for the complete MAD experiment required about seven hours.

The software package SOLVE was used to perform phase determination and assess the quality of their MAD experiment. The SOLVE package offered several advantages for them. Whereas manual solution of Patterson maps in high symmetry space groups with multiple heavy atom sites is challenging and time consuming, SOLVE offered a simple-to-set-up, automatic phase determination alternative. The three-wavelength unmerged data with Bijovet pairs were input to SOLVE. Using the anomalous and dispersive differences between datasets, SOLVE determined a single solution for four of five Se-Met sites within 78 minutes running on a 500Mhz DC ALPHA workstation. SOLVE was even able to distinguish the correct hand of the structure. The time from placing the crystal into the beam until the structure was solved was an astonishing 11 hours.

The initial electron density maps were easily interpretable (Figure I-2). The map quality was then improved through solvent-flattening and histogram-matching routines using the program "dm" in the CCP4 program suite. The solvent-flattened map could be unambiguously traced for 98 of 154 residues. After refinement using XPLOR, the amino acids originally traced were returned in the 2Fo-Fc map and more importantly, most of the remaining residues could be traced. Their current 2.0 Å model includes residues 3 to 154 and 40 water molecules (R=26.3%, R_{free}=33.7%). ■

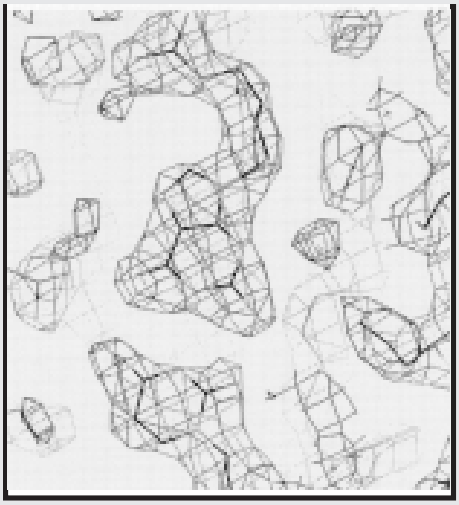

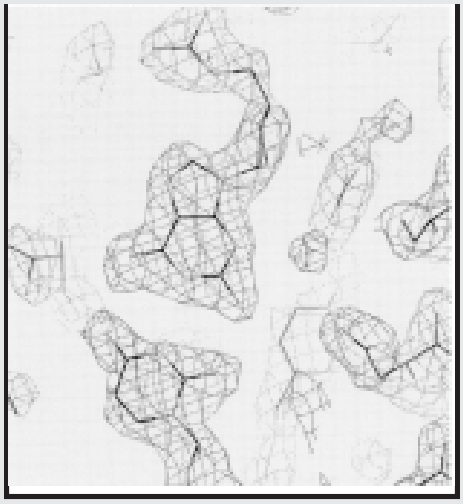

Figure I-3:
(left)
Experimental MAD electron density from Se-MET phasing.
(right)
Electron density from phases after refinement of the structure.

Soft X-Ray Emission Spectroscopy (X1B)

K. Smith *et al.* (Boston U.)

1997 saw the commissioning by Kevin Smith's group from Boston University of a new high resolution soft x-ray emission spectrometer on X1B. There are only a handful of such instruments around the world, and this is the only one dedicated for use at the NSLS. Soft x-ray emission (SXE) spectroscopy allows the bulk electronic structure of complex solids to be measured without regard to the quality or cleanliness of the solid surface. In particular, SXE allows the elementally resolved partial density of states to be measured. SXE also allows the direct measurement of hybrid states, of d-d excitations in transition metal systems, and of changes in electronic structure during metal to non-metal transitions while the sample is in applied electric or magnetic fields.

The BU group is using the spectrometer in the study of three different classes of materials: wide band gap nitride semiconductors, organic superconductors, and transition metal oxides. During two runs in 1997, the BU group calibrated their SXE instrument and began study of each of these materials systems. As an example of the first experiments, Figure I-4 shows a series of N *K*-emission spectra from the $Al_xGa_{1-x}N$ alloy system. Owing to the magnitude of the bandgap in these materials, they are ideal candidates for optoelectronic devices working in the blue/UV range of the electromagnetic spectrum. The spectra in Figure I-4 are the result of tuning the incident photon energy to just above the N *K* absorption edge, thus creating holes on the N *1s* level, and measuring the radiative decay of these holes. Dipole selection rules imply that the resulting spectra correspond to the N *2p* partial density of states (PDOS). Thus these spectra show the behavior of the dominant part of the valence band density of states in $Al_xGa_{1-x}N$ as the Al content is varied. The band gap for $Al_xGa_{1-x}N$ varies from 6.2 eV in AlN (x = 1) to 3.4 eV in GaN (x = 0). The motion of the top of the valence band is clearly visible in the spectra, shifting linearly by 1.5 eV as x varies from 0 to 1. This indicates

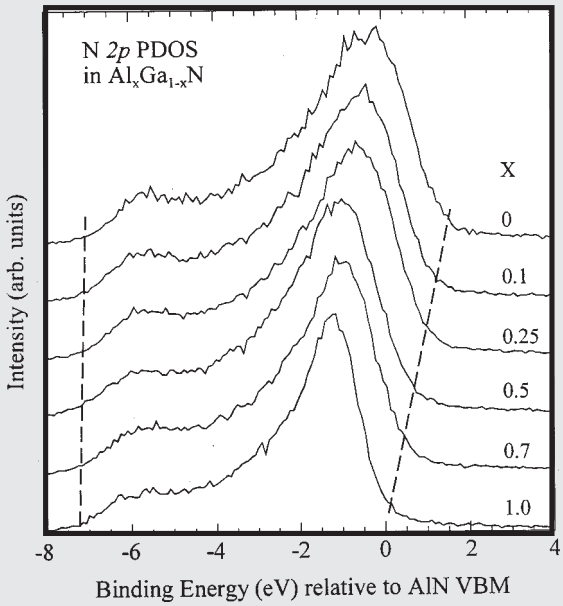

Figure I-4: A series of N *K*-emission spectra from the $Al_xGa_{1-x}N$ alloy system as a function of Al content x ($0<x<1$), excited with a photon energy just above the N *K* absorption edge. The binding energy range shown (0-10 eV) covers the valence bands.

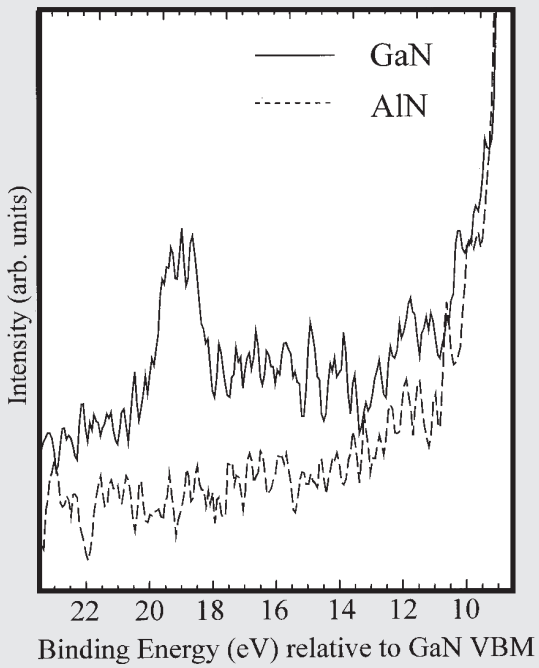

Figure I-5: Same as Figure I-1, except at greater binding energy (14-24 eV).

essentially a symmetric opening up of the band gap. Unlike photoemission, there are no charging problems associated with such measurements, and the surfaces of the films were not atomically cleaned. A further illustration of the power of this spectroscopy is presented in Figure I-5. Here the N *K*-emission spectra below the valence band are shown. Clearly visible at 19 eV is a well defined emission feature. This is direct observation of N *2p* states hybridized with the Ga *3d* shallow core level. The interatomic Ga *3d* - N *1s* transition is forbidden, so the emission to the *1s* hole must arise from states with N *2p* character. That the emission at 19 eV is due to these hybrid states is proven by the reduction of the emission with Al content.

Other experiments in the first runs explored the spatially resolved electronic structure of organic superconductors, and changes in *d-d* transitions in transition metal oxides during metal to non-metal transitions. ■

Fermi Surface Mapping in Photoemisson

P.D. Johnson, T. Valla, and A.V. Fedorov (BNL Physics Department)

Photoemission represents one of the most powerful techniques for the study of the electronic structure of materials. It has seen widespread application to the study of metals, superconductors, surfaces, thin films and, in its spin-resolved form, magnetic systems. In recent years, the development of higher energy resolution in this technique has allowed important contributions to be made to the field of high temperature superconductivity.

Recently, a group in the Physics Department at BNL has commissioned a new photoemission facility based on the use of a Scienta hemispherical analyzer. This instrument has the capability of measuring simultaneously the photoelectron's energy and angle of emission over a wide range of angles. An ultimate energy resolution of 5 meV and an angular resolution of ≤0.2°are anticipated. The momentum resolution of the system is demonstrated in Figure I-6(a) where we show the experimentally observed electronic bands of molybdenum dispersing through momentum space in the NH direction of the Brillouin zone. The experimental observations are compared with a tight-binding calculation of the band structure in the same region of the zone. The spectral density plot is obtained with incident photons of energy 390 eV produced by the soft X-ray undulator on the X1B beamline. The center of electron emission corresponds to an angle of 15° with respect to the surface normal. The experimental parallel momenta, $k_{||}$, are determined from $k_{||} = 0.5123\ (E_{kin})^{0.5} \sin\phi$, where E_{kin} represents the photoelectron's kinetic energy above the vacuum level and j the angle of emission. By using higher incident photon energies, the variation in $k_{\perp}$ of the final state as a function of $k_{||}$ is greatly reduced. However, the question arises as to whether, at these energies, it will still be possible to observe the momentum dependence of the electronic structure. That one can in fact do so is clear from Figure I-6(a). An important point to note is that the experimental observations are obtained with no changes in the voltages applied to the analyzer. One is simply "opening the shutter and taking a picture" of this particular section of the Brillouin zone. In Figure I-6(b)

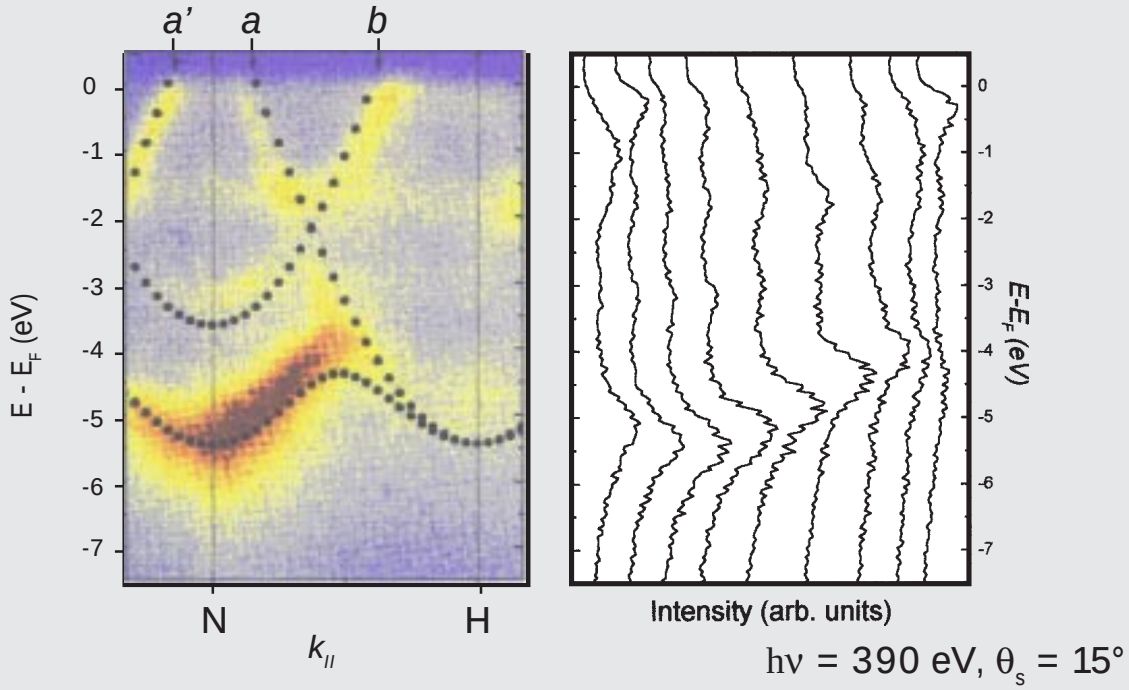

Figure I-6: (a) Spectral density plot recorded from a Mo(110) surface along the NH section of the Brillouin zone. The incident photons from beamline X1B have an energy of 390 eV and the center angle of emission corresponds to 15°. The dotted lines indicate the results of a tight-binding calculation of the electronic structure in the same region of the zone.
(b) Cuts through the spectral density plot of Figure I-6(a) to produce conventional angle-resolved photoemission spectra in the NH direction.

we show for comparison cuts through Figure I-6(a) at well defined spacings in angle in order to provide the traditional angle-resolved photoemission spectra.

A spectral density plot, as shown in Figure I-6(a), allows us to examine in detail the Fermi surface of the material under investigation. This Fermi surface is defined by the points in momentum space at which the electronic bands intersect the Fermi level E_F. Thus, the points labeled a and a' in Figure I-6(a) correspond to calipers on an ellipse centered at the N point of the Mo Fermi surface. An interesting observation is that the tunability of synchrotron radiation and the symmetry of the crystal allow the entire surface of such an ellipse to be mapped out without rotating the azimuth of the crystal.

A measurement of the calipers, or spanning vectors, on the Fermi surface of a material is important for our understanding of the oscillatory exchange coupling that is observed in magnetic multilayers. Indeed, Figure I-7 [1] shows a calculation of the Fermi surface of bulk molybdenum and indicates the relevant spanning vectors for a multilayer grown in the (110) direction with molybdenum as a spacer layer. For comparison, we indicate in Figure I-7 the points a, a', and b corresponding to the same points in Figure I-6(a). Interestingly, the experimental determination in Figure I-6(a) of the spanning vector q from a to b would result in an oscillatory period length, $2\pi/q$, 80% of that indicated in the theoretical calculation represented in Figure I-7. ■

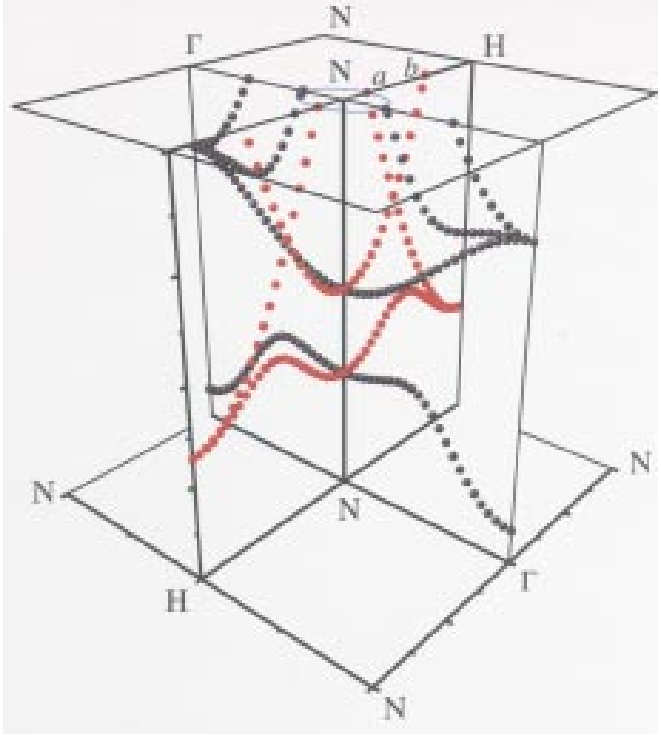

Figure I-7: Calculated Fermi surface of Mo showing the spanning vectors appropriate to oscillatory coupling in the (110) direction from Ref. [1].

[1] M.D. Stiles, *Phys. Rev. B* 48, 7238 (1993).